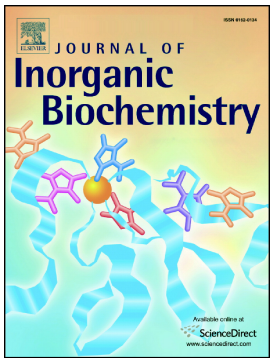

Influence of the introduction of a mitochondrion-targeting group on the anticancer activity of a copper complex

Sen Li, Jin'an Zhao, Yan Guo, Yameng Mei, Bangpeng Yuan, Ning Gan, Junshuai Zhang, Jiyong Hu, Hongwei Hou

PII: S0162-0134(20)30130-6

DOI: https://doi.org/10.1016/j.jinorgbio.2020.111102

Reference: JIB 111102

To appear in: *Journal of Inorganic Biochemistry*

Received date: 15 January 2020

Revised date: 29 April 2020

Accepted date: 30 April 2020

Please cite this article as: S. Li, J. Zhao, Y. Guo, et al., Influence of the introduction of a mitochondrion-targeting group on the anticancer activity of a copper complex, *Journal of Inorganic Biochemistry* (2018), https://doi.org/10.1016/j.jinorgbio.2020.111102

Influence of the Introduction of a Mitochondrion-targeting Group on the Anticancer Activity of a Copper Complex

Sen Li[b], Jin'an Zhao[a,*], Yan Guo[a], Yameng Mei[b], Bangpeng Yuan[b], Ning Gan[a], Junshuai Zhang[a], Jiyong Hu[a] and Hongwei Hou[b]

[a]College of Material and Chemical Engineering, Henan University of Urban Construction, Pingdingshan 467036 Henan, P. R. China.

[b]College of Chemistry, Zhengzhou University, Zhengzhou 450001 Henan, P. R. China.

Corresponding Author

Jin'an Zhao

Address: College of Material and Chemical Engineering, Henan University of Urban Construction, Pingdingshan 467036 Henan, P. R. China.

Email: zjinan@zzu.edu.cn

Abstract

Mitochondria participate in multiple cellular functions, including in particular energy production and cell apoptosis, and targeting mitochondria might enhance the efficiency of chemotherapeutic agents. Triphenylphosphine (TPP) is a commonly used mitochondrion-targeting group, so two copper complexes, Cu(2-pbmq)(CH_3OH)Br_2 (**1**) and [Cu(2-pbmq)(TPP)Br]$_2$ (**2**) were designed, synthesized, and characterized by X-ray crystallography, (2-pbmq = 2-((2-(pyrazin-2-yl)-1H-benzo[*d*]imidazol-1-yl)methyl))quinoline), to investigate the influence of the mitochondrion-targeting group on the anticancer activity of the metal complex. Although the presence of the TPP group diminished the intensity of the interaction properties of the complex with DNA, the *in vitro* anticancer activity and cellular uptake of the TPP-containing complex were markedly superior to those of its TPP-lacking counterpart. Detailed studies on the more potently cytotoxic complex **2** revealed that it arrested

the cell cycle at the G0-G1 phase, causing mitochondrial dysfunction, involving the potential simultaneous mitochondrial membrane collapse, cellular ATP leave depletion, and Ca^{2+} leakage from the mitochondria, eventually inducing cell apoptosis. In summary, the introduction of a mitochondrion-targeting group enhances the biological activity and cytotoxicity of the complex.

Keywords: *Mitochondria-targeting; Triphenylphosphine; Copper complexes; Anticancer; Apoptosis*

1. Introduction

Mitochondria are considered prime targets of metal complexes with anticancer activity [1]. These subcellular organelles are present in most eukaryotic cells and are generally recognized as "the cell powerhouses" [2]. Mitochondria also have a key role in regulating cell death [3]. Mitochondrion-targeting metal complexes can disturb the function of mitochondria and may trigger extensive ATP depletion, leading to the death of cancer cells [4].

Currently, the TPP group is regarded as a pharmacophore of interest, as its induction is regard as an effective approach to delivering agents to mitochondria [5]. As a functional targeting group, TPP has been extensively studied in the context of the design and synthesis of metal complexes, most of which have excellent potential in chemotherapy, as they influence mitochondrial metabolism. For instance, Guo's research group recently reported a triphenylphosphonium-modified terpyridine platinum(II) complex, TTP, which exhibited marked cytotoxicity and exerted strong inhibition of both mitochondrial and glycolytic bioenergetics, inducing cancer cells to enter a hypometabolic state [6]. In addition, platinum, ruthenium, and gold complexes containing TPP were designed and synthesized by other group to investigate the effect that the TPP targeting group had on metal complexes' bioactivity and cytotoxicity [7–11]. In contrast to the mentioned metallic elements, copper is an endogenous and readily available metal. It is also physiologically essential and characterized by low toxicity. In fact, copper is involved in many biological processes taking place in the human body [12–14]. Some copper complexes comprising TPP have been reported to target mitochondria and

adversely affect mitochondrial metabolism [15–18]. Notably, the rational choice of the axial organic scaffold offers an approach to the fine-tuning of the pharmacological properties of metal complexes with high anticancer activity. The benzimidazole and quinolone organic scaffolds are a good choice for synthesizing anticancer chemotherapeutics, given their extensive biological properties, including their antiviral, anticancer, antibacterial, and antifungal activities [19–21]. Our group investigated two copper complexes, dinuclear $[Cu(qbm)Cl_2]_2$ and mononuclear [Cu(qbm)Br(TPP)] (qbm=2-(2'-quinolyl)benzimidazole), and found that the complex bearing the TPP ligand is superior to the other one in terms of reactivity and cytotoxicity. Additionally, [Cu(qbm)Br(TPP)] was observed to cause dual mitochondrial and nuclear DNA damage [22].

Our persisting research interest in metal complexes with anticancer activity led us to explore the effect that the TPP targeting group has the cytotoxicity and mitochondrial damage properties of the said complex. In the present study, complexes **1** and **2** were synthesized, and their *in vitro* anticancer activities were investigated. The insight we garnered through these investigations may provide the basis for a promising strategy for the functional modification of metal complexes aimed at enhancing their anticancer activity.

2. Experimental section

2.1. Materials and instruments

GelRed (Biotium, USA), pBR322 DNA (TaKaRa Biotechnology Ltd, China), calf thymus DNA (CT-DNA, Sigma Aldrich, USA), dimethyl sulfoxide (DMSO, Sigma Aldrich, USA) (3-(4,5-dimethylthiazol-2-yl)-2,5-diphenyltetrazolium bromide (MTT, Sigma Aldrich, USA), Fluo-3 acetoxymethyl ester (Fluo-3/AM, Sigma Aldrich, USA), ethidium bromide (EB, Sigma Aldrich, USA), cisplatin (Shanghai Energy Chemical Ltd, China), fetal bovine serums (FBS, Hyclone Laboratoreis Inc, USA). All the experimental reagents involved in this study were purchased from commercial sources and used as received without further purification treatment. $CuBr_2$, CuBr, 2-(bromomethyl)isoquinoline, 1,2-diaminobenzene, 2-pyrazinecarboxylicacid were purchased from Bide Pharmatech Ltd (China). TPP was purchased from J&K Scientific

Ltd (China). Mitochondrial membrane potential assay kit, enhanced ATP assay kit, and the cell mitochondria isolation kit were purchased from Beyotime (China). Annexin V-FITC apoptosis detection kit was purchased from BD Bioscience (USA). Buffer solutions (5 mM Tris-HCl/50 mM NaCl; pH = 7.4 and 50 mM Tris-HCl/50 mM NaCl; pH = 7.4; TAE buffer (40 mM Tris, 20 mM acetic acid, and 1 mM EDTA, pH = 8.3).) for the related biological experiments was prepared using double distilled water.

Infrared spectra (IR) with KBr discs were recorded on a PerkinElmer Fourier transform-IR spectrometer (Perkin Elmer, Waltham, MA, USA) in the 400–4000 cm^{-1} range. Electrospray ionization mass spectra (ESI-MS) were measured on a Thermo Scientific LCQ fleet ESI-MS spectrometer. Microanalysis (C, H, and N) was carried out using Flash EA 1112 elemental analyzer (Thermo Fisher Scientific, Waltham, MA, USA). UV-Vis absorption spectra were measured by a Specord 200 UV-Vis spectrophotometer (Analytik Jena, Germany). MOS-500 instrument (Bio-Logic Science Instruments, Seyssinet-Pariset, France) was used in circular dichroism spectral analysis. Tecan Infnite M1000 Pro microplate reader (Tecan, Morrisville, NC, USA) was used in MTT assay, adenosine triphosphate (ATP) production assay, and EB replacing experiment to read the chemiluminescence or absorbance. ICP-MS Nex-ION 300X instrument (PerkinElmer, USA) was used in cell uptake assay. Double distilled water was obtained using a Milli-Q® water purification system (Millipore) for all related experiments. Flow cytometric analysis was done using a BD LSRFortessaTM Cell Analyzer (BD Biosciences, USA). DNA images were captured on a G: BOX F3 gel imaging system (Syngene, UK).

2.2. Synthesis of ligand and its corresponding complexes

The route for the synthesis of the ligand and its counterpart complexes was presented in **Scheme 1**.

2.2.1. Synthesis of ligand (2-pbmq)

2-((2-(pyrazin-2-yl)-1H-benzo[*d*]imidazol-1-yl)methyl)quinoline (2-pbmq) was prepared by the substitution reaction between 2-(pyrazin-2-yl)-1H-benzo[d]imidazole (1 mmol, 0.196 g) and

2-(bromomethyl)isoquinoline (1 mmol, 0.221 g) in acetone solution. After the reaction heated to 60 °C and refluxed 12 h and slowly cooled to room temperature, ashen powder-shaped ligands were obtained. IR (KBr/pellet, cm^{-1}): 3400 (w), 3053 (m), 1598 (m), 1505 (m), 1445 (w), 1414 (s), 1168 (m), 1117 (s), 1015 (s), 977 (m), 742 (m), 616 (w).

2.2.2. Synthesis of the complex Cu(2-pbmq)(CH_3OH)Br_2 (1)

2-pbmq (0.02 mmol, 0.0067 g) dissolved in methanol (3 mL) was added to a solution of $CuBr_2$ (0.02 mmol, 0.0045 g) in ethanol (2 mL), which placed together in a sealed glass container at 25 °C. After one week, the brown crystals were isolated to give complex **1**. Yield: 81%, based on Cu. Elemental Analysis (%) calcd. for $C_{22}H_{19}Br_2CuN_5O$: C, 44.58; H, 3.23; N, 11.81; found (%): C, 44.63; H, 3.24; N, 11.93. ESI-MS (Found, m/z): 558.83 [Cu(2-pbmq) Br_2 + H]$^+$, (Calcd. m/z: 558.90). IR (KBr/pellet, cm^{-1}): 3434 (m), 3062 (m), 1616 (m), 1566 (w), 1506 (m), 1479 (s), 1453 (s), 1389 (m), 1180 (m), 1125 (m), 1038 (s), 753 (s), 517 (w), 478 (w).

2.2.3. Synthesis of the complex [Cu(2-pbmq)(TPP)Br]$_2$ (2)

A mixture solution (7 mL) containing CuBr (0.03 mmol, 0.0043 g,), 2-pbmq (0.01 mmol, 0.0034 g), TPP (0.02 mmol, 0.0052 g), acetonitrile (4 mL), and dichloromethane (3 mL) stirred at room temperature to obtain a yellow solution. The resulting mixture solution was left to stand at 25 °C about two weeks, and the yellow crystals were obtained. Yield: 61%, based on Cu. Elemental Analysis (%) calcd. for $C_{78}H_{60}Br_2Cu_2N_{10}P_2$: C, 63.03; H, 4.07; N, 9.42; found (%): C, 62.89; H, 4.06; N, 9.68. ESI-MS (found, m/z): 662.25 [Cu(2-pbmq)(TPP)]$^+$, (calcd. m/z: 662.13). IR (KBr/pellet, cm^{-1}): 3434 (w), 3061 (m), 1598 (m), 1503 (m), 1479 (m), 1433 (s), 1331 (s), 1150 (s), 1017 (m), 824 (m), 748 (s), 696 (s), 608 (w).

2.3. X-ray crystallography determination

Crystals of complexes **1** and **2** qualified for X-ray analyses were obtained by solvent evaporation method. X-ray diffraction measurements were performed on a Super Nova diffractometer with Cu-Kα radiation (λ = 1.54184 Å) at 293 K or 160 K. The structures were

solved and expanded utilizing both direct method and Fourier technology. The analyses of complexes were obtained with SHELXL 2018 and the OLEX2 crystallographic programs [23–24]. All the non-hydrogen atoms were refined anisotropically [25]. The structures were plotted by using crystal maker. The crystallographic and structure parameters of the complexes were shown in the **table 1**. The data related to the main bond lengths and bond angles were shown in the **table 2**.

2.4. Thermogravimetric assay and solution stability determination

A model TGA/SDTA 851 MOD thermal analyzer was used to record simultaneous thermogravimetric curves at a heating rate of 10 °C min^{-1} over the temperature ranging from room temperature to 900 °C in a flowing nitrogen atmosphere of 20 mL/min using platinum crucibles. Complexes **1** and **2** were dissolved in buffer solutions (5 mM Tris-HCl/50 mM NaCl; pH = 7.4) at 5×10^{-5} M concentration. UV-Vis absorption spectra of the complexes **1** and **2** were recorded on a Specord 200 UV-Vis spectrophotometer (Analytik Jena, Germany) in different time intervals.

2.5. DNA interaction properties assays

2.5.1. Circular dichroism spectral analysis

CT-DNA concentration was measured by UV-Vis at 260 nm and 280 nm with a molar absorption coefficient 6600 M^{-1} cm^{-1} [26]. The value of A_{260}/A_{280} was located in 1.8–1.9, which illustrated that the DNA solution was free of protein sufficiently [27–28]. CT-DNA (50 μM) was incubated with various concentrations of complexes **1** and **2** (10–50 μM) in the buffer solution (5 mM Tris-HCl/50 mM NaCl buffer pH = 7.4) at room temperature. The mixture solutions were measured immediately in MOS-500 instrument (Bio-Logic Science Instruments, Seyssinet-Pariset, France) and recorded scanning wavelength ranging from 220 nm to 320 nm. The background of the buffer solution was deducted before testing.

2.5.2. EB replacing experiment

CT-DNA (100 μM)/EB (10 μM) system was incubated in a 96-well cell culture plate for 1 h at 37 ºC. And then the mixture solutions were titrated by complexes **1** and **2** ranging from 0 to 90 μM in constant temperature incubator at 37 ºC for 4 h. The fluorescence spectra were measured on Tecan Infnite M1000 Pro microplate reader (Tecan, Morrisville, NC, USA) (λ_{ex} = 490 nm; λ_{em} = 510–800 nm).

2.5.3. DNA cleavage

pBR322 DNA was incubated with various concentrations of complexes **1** and **2** (10–50 μM) in buffer solution (50 mM Tris-HCl/50 mM NaCl; pH = 7.4) at 37 °C for 4 h. DNA samples were analyzed by electrophoresis (85 V, 1 h) on a 1% agarose gel in 1×TAE buffer (40 mM Tris, 20 mM acetic acid, and 1 mM EDTA, pH = 8.3). The image was captured on a G: BOX F3 gel imaging system (Syngene, UK).

2.6. *In vitro* anticancer activities

2.6.1. Cell lines and culture conditions

Human cancer and normal cells: BGC823 (gastric cancer cell line), TFK-1 (cholangio carcinoma cell line), SMMC7721 (liver cancer cell line), L-02 (normal liver cell line). L-02 and BGC823 cells were maintained in Dulbecco's modified Eagle's medium (DMEM) at 37 °C under 5% CO_2, 95% air in a humidified incubator. TFK-1 and SMMC7721 cells were maintained in Roswell Park Memorial Institute (RPMI) 1640 medium at 37 °C under 5% CO_2, 95% air in a humidified incubator.

2.6.2. Cytotoxicity assay

The cytotoxicity of the tested complexes towards BGC823, TFK-1, SMMC7721, L-02 cell lines was determined by MTT assay. When cells cultured in 96-well cell culture plate were grown to confluence, various concentrations of the complexes, cisplatin, and 2-pbmq were

added for 48 h at 37 °C under 5% CO_2, 95% air in a humidified incubator. The treated cells were labeled with 20 μL MTT dye (5 mg/mL) for 4 h. The culture medium was sucked out and DMSO was added (150 μL per well). The 96-well cell culture plate was shaken for 10 min. The absorbance values at 492 nm were measured using a Tecan Infnite M1000 Pro microplate reader (Tecan, Morrisville, NC, USA).

2.6.3. Lipophilicity and cellular uptake

The lipophilicity (log $P_{O/W}$) of complexes **1** and **2** was measured in a water/1-octanol system using the shake-flask method. Solutions of complexes **1** and **2** (30, 40, and 50 μM) were prepared in water presaturated with 1-octanol. Equal volumes (2.0 mL) of the solution and 1-octanol presaturated with water were mixed and shaken at room temperature for 24 h and then separated into two phases by centrifugation. The concentration of the solute in the aqueous phase was determined by spectrophotometry. The log *P* values were calculated from the average of three independent measurements. The log $P_{O/W}$ value was calculated using the equation

$$\log P_{O/W} = \log[([C]_{initial}-[C]_{final})/[C]_{final}]$$

Inductively coupled plasma mass spectrometry (ICP-MS) was used to measure the intracellular Cu contents. SMMC7721 cells were seeded in 100 mm cell culture plate to welt. After 24 h, SMMC7721 cells were treated with complexes **1** and **2** at 10 μM for 8 h. And then cells were collected with trypsin and washed with PBS in centrifuge tubes. The cytoplasm, nucleus, and mitochondria of SMMC7721 cells were isolated by a cell mitochondria isolation kit according to the manufacturer's instruction. The collected extractions were digested with HNO_3 (100 μL) at 95 °C for 1 h, H_2O_2 (30%, 50 μL) at 95 °C for 1 h, and HCl (100 μL) at 95 °C for 1 h, sequentially. The solutions were then diluted to a final volume of 4 mL with double distilled water. The Cu contents were calculated as ng Cu per 10^6 cells.

2.7. Cell death mechanism studies

2.7.1. Annexin V-PI assay

SMMC7721 cells were cultured in 6-well cell culture plate to welt for 24 h and then treated with complex **2** at the indicated concentrations for 24 h. The SMMC7721 cells were collected and stained using an Annexin V-FITC apoptosis detection kit (BD) according to the manufacturer's instruction. SMMC7721 cells were collected by using flow cytometry. Cells at different stages were analysed by FlowJo software.

2.7.2. Cell cycle assay

SMMC7721 cells were cultured in 6-well cell culture plate to welt for 24 h. Then culture mediums were replaced by the fresh mediums containing various concentrations of complex **2** for 8 h. The cells were washed with PBS and digested with trypsin and immobilized with 70% ice-cold ethanol, and eventually preserved at 4 ºC. The immobilized cells were disposed according to the manufacturer's instruction of KeyGEN Cycle Test Plus DNA reagent kit. The cells were collected by flow cytometry and data were analyzed by ModFit LT Software.

2.7.3. Measurement of mitochondrial membrane potential

The mitochondrial membrane potential assay was performed using mitochondrial membrane potential assay kit according to the manufacturer’s instruction (Beyotime, China). SMMC7721 cells were cultured in 6-well cell culture plate to welt for 24 h. After incubated with specified concentrations of complex **2** at 37 ℃ for 8 h, the cells were washed with PBS and digested with trypsin and collected in different centrifuge tubes. The cells were further incubated with 1 mL Rh123 working solution for 20 min at 37 ºC in dark before rinsed and centrifuged three times with RPMI 1640 medium without FBS. The cells were measured by flow cytometry. Data were analyzed by FlowJo Software.

2.7.4. ATP production assay

The ATP concentrations were performed using enhanced ATP assay kit (Beyotime, China) according to the manufacturer's instruction. The standard curve was obtained by the known

concentrations of standard ATP sample. SMMC7721 cells were incubated in 6-well cell culture plate to welt for 24 h. The cells were incubated with various concentrations of complex **2** at 37 °C for 24 h. After incubated, the cells were lysed and collected in centrifuge tubes and centrifuged in 12000 g for 5 min at 4 °C and only reserved supernatant. 100 μL ATP working solutions were added to the 96 round black well plate for 5 min before reserved supernatant were added to the 96 round black well plate. The luminescence was measured using a Tecan Infinite M1000 Pro microplate reader (Tecan, Morrisville, NC, USA).

2.7.5. Intracellular Ca^{2+} generation assay

Fluo-3/AM (Sigma Aldrich, USA) staining method was used to measure the intracellular Ca^{2+} concentration. SMMC7721 cells were cultured in 6-well cell culture plate to welt for 24h. After SMMC7721 cells treated with complex **2** at indicated concentrations for 8 h, the cells were washed with PBS and incubated with 1 mL Fluo-3/AM working solution for 30 min at 37 ºC in dark. Lastly, the cells were washed with PBS and collected, and fleetly analyzed by flow cytometry. Data were analyzed by FlowJo Software.

3. Results and discussion

3.1. Crystal structure

Complex **1** crystallizes in a triclinic crystal system and *P*-1 space group. As illustrated by the structure depicted by **Fig. 1**, the complex's asymmetric unit consists of one Cu^{2+} ion, one neutral ligand, one coordinated methanol molecule and two bromine atoms. In five-coordinated complexes, the geometry index, τ_5, can be used to discriminate between structures characterized by the square pyramidal and trigonal bipyramidal geometries. The τ_5 value for complex **1** was determined to be 0.27, by performing a calculation utilizing the values for the N(2)-Cu(1)-Br(2) (163.22(8)°) and N(1)-Cu(1)-Br(1) (147.03(7)°) angles. Importantly, a τ_5 value of 1.00 identifies a structure with an ideal trigonal bipyramidal geometry, whereas a value of 0.00 identifies a structure with an ideal square pyramidal geometry [29]. In complex **1**, the

coordination geometry around the Cu center can be described as distorted tetragonal pyramidal. The Cu–N bond lengths are similar to each other: the Cu(1)–N(1) = 2.071(3) Å and Cu(1)–N(2) = 1.991(3) Å. Although the crystal structures of complexes **2** and **1** are characterized by the same crystal system and space group, the coordination mode of the Cu center of complex **2** is different from its counterpart of complex **1**. In four-coordinated complexes, the geometry index τ_4 can be used to discern between a square planar and a tetrahedral geometry. The τ_4 value for complex **2** was determined to be 0.92, by performing a calculation utilizing the values for the P(1)-Cu(1)-Br(1) (118.019(16)°) and Br(1)-Cu(1)-Br(1a) (112.387(15)°) angles. Notably, with regard to τ_4, a value of 1.00 identifies a structure with an ideal tetrahedral geometry, a value of 0.00 identifies a structure with an ideal square planar geometry and a value of 0.85 identifies a structure with an ideal trigonal pyramidal geometry [30]. The distorted tetrahedral coordination around the Cu center of complex **2** comprises two bromine atoms, the N atom of a terminally bound ligand, and the P atom of TPP. Additionally, a μ_2-Br group acts as bridge between Cu(1) and Cu(1a). The distance between Cu(1) and Cu(1a) is 2.7896(5) Å. In complex **2**, the ligands coordinating Cu(1) and Cu(1a) lie on two essentially parallel planes (2-(pyrazin-2-yl)-1H-benzo[*d*]imidazole and isoquinoline planes). The values for the bond lengths and bond angles determined for complex **2** are within the normal range for similar Cu(I) complexes [31].

3.2. Stability determination

As illustrated by the data reported in **Fig. S1**, complexes **1** and **2** are relatively stable, and the integrity of their crystals is maintained up to at least 200 °C. In complex **1** the unit cell includes disorder, which was observed from the difference Fourier maps. In the case of complex **1**, a 5.69% weight loss observed to occur as the temperature rose from 50 to 200 °C, which was ascribed to the loss of solvent molecules.

In order to conduct investigations on the anticancer activity of a complex, the stability of the said complex under physiological conditions is necessary. The UV-Vis absorption spectra of complexes **1** and **2** recorded at different time intervals are reported in **Fig. S2**, no obvious

change was observed in the spectra of complexes **1** and **2** over a 48 h period, indicating that these complexes were almost completely stable in solution.

3.3. DNA interactions

3.3.1. Circular dichroism spectral analysis

DNA is the primary intracellular target for anticancer metal complexes [32]. The interaction of the complexes with CT-DNA was investigated by circular dichroism spectrometry. The characteristic peaks of B-DNA consist of a positive and a negative band at 275 nm and 245 nm, which are due to base stacking and the B-conformation of DNA, respectively [33]. As can be evinced from the spectra reported in **Fig. 2**, in the presence of complexes **1** and **2**, the typical bands of B-DNA underwent red-shifts and their intensities were significantly reduced, indicating that both complexes can interact with DNA. Furthermore, the spectral modifications associated with the presence of complex **2** were stronger than their counterparts observed for complex **1**, indicating that complex **2** causes a stronger perturbation of DNA's secondary structure.

3.3.2. EB competition binding assay

The DNA binding properties of complexes **1** and **2** were further studied by conducting EB competition binding assays to quantify the complexes' binding affinity for DNA. As can be evinced from the data in **Fig. 3**, as increasing amounts of complexes **1** and **2** are added to the EB-DNA solution, a dramatic hypochromism effect was observed at 612 nm. The classical linear Stern-Volmer equation: $I_0/I = 1 + K_{sv}[Q]$, where I_0 and I are the fluorescence intensities in the absence and presence of a quencher, respectively, and [Q] is the quencher concentration. K_{sv}, the linear fit plot of I_0/I *versus* [Q], represents the Stern-Volmer dynamic quenching constant [34]. K_{app}, the apparent DNA binding constant, was calculated *via* the following equation: K_{EB} [EB] = K_{app} [complex]. Herein $K_{EB} = 1.0\times10^7$ M^{-1} and [EB] = 10 μM. Notably, K_{EB} is the binding constant of EB to DNA, and [complex] is the concentration of the complex in the situation whereby a 50% reduction in the fluorescence intensity of EB is observed. The

approximate values for K_{sv} and K_{app} were calculated to be 1.10×10^4 M^{-1} and 1.79×10^7 M^{-1}, in the case of complex **1** and 1.26×10^3 M^{-1} and 1.73×10^6 M^{-1}, respectively, in the case of complex **2**, demonstrating that complex **1** displayed a stronger affinity for DNA than complex **2**. All in all, the results of EB competition binding assays in combination with circular dichroism spectrometry data indicated that complexes **1** and **2** may bind to DNA *via* intercalation.

3.3.3. Agarose gel electrophoresis assays

The interaction of complexes **1** and **2** with pBR322 DNA was investigated conducting agarose gel electrophoresis assays. pBR322 DNA can present itself in three forms: supercoiled (Form I), nicked/open circular (Form II) and linear (Form III). As can be evinced from the electrophoresis assay results reported in **Fig. 4**, in the presence of an endogenous biological oxidation-reduction agent (H_2O_2 or ascorbic acid), the treatment of pBR322 DNA with complexes **1** and **2** resulted in the gradual conversion of the Form I into Forms II and III. Complexes **1** and **2** displayed strong DNA cleavage activity, and DNA was cleaved by complex **1** to a greater extent than by complex **2**.

3.4. *In vitro* anticancer activities

3.4.1. Cytotoxicity analysis

The *in vitro* toxicity of complex **1**, complex **2**, and 2-pbmq against SMMC7721, BGC823, TFK-1, and L-02 cells were determined performing the MTT assay over a 48 h period. The IC_{50} values thus determined are reported in **Table 3.** Treatment of cells with 2-pbmq alone does not affect cell viability, even at 100 μM concentration [35]. Complex **1** exhibited medium cytotoxicity against the tested cancer cell lines. Complex **2**, on the other hand, showed marked cytotoxicity against the same cancer cell lines. The *in vitro* anticancer activity of the tested compounds decreased in the following order: **2** > cisplatin > **1** > 2-pbmq. The enhanced anticancer activity of complex **2** may result from the introduction of the ancillary ligand-TPP, which, as indicated by the results of the experiments described in the next section, increased the

relative lipophilicity of the copper complex [36–37].

3.4.2. Cellular uptake and lipophilicity

The cellular uptake properties of metal-based anticancer agents have an effect on the anticancer activity of the said agents. Consequently, the cellular uptake ability of complexes **1** (10 μM) and **2** (10 μM) in SMMC7721 cells were assessed *in vitro* implementing the ICP-MS assay. As can be evinced from the data reported in **Fig. 5**, under the same conditions, the cellular uptake of complex **2** (109.28 ± 5.46 ng per 10^6 cells) was greater than that of complex **1** (18.48 ± 0.80 ng per 10^6 cells). Furthermore, compared to complex **1**, complex **2** was mainly distributed in the nucleus. Additionally, the copper content of the mitochondria following treatment with complex **2** (8.34 ± 0.34 ng per 10^6 cells) was approximately three times higher than that observed after the treatment with complex **1** (2.64 ± 0.07 ng per 10^6 cells). This difference may be the result of the introduction of the mitochondrion-targeting group. The lipophilicity (log $P_{o/w}$) of complex **2** was determined by the shake–flask method to be 1.24 in a water/1-octanol system (**Table 4.**), a substantially larger value than that determined for complex **1** (0.46), which suggests that complex **2** has a greater tendency to penetrate the phospholipid bilayers than complex **1**. The results of the cellular uptake and cytotoxicity experiments detailed above may be positive correlation with lipophilicity of the complexes. Since complex **2** exhibited significant cytotoxicity and high uptake by SMMC7721 cells, we were prompted to further explore the possible anticancer mechanism of this complex.

3.5. Cell death mechanism studies

3.5.1. Cell apoptosis

The Annexin V-PI assay was implemented to test whether apoptosis was involved in complex **2**-induced cell death. As can be evinced from the data reported in **Fig. 6**, the percentage of early and late apoptotic cells increased in a dose-dependent manner after SMMC7721 cells were treated with complex **2**. After being treated with various concentrations of complex **2** (0, 1.5, 3,

and 4.5 μM) for 24 h, the percentage of cells in the early and late apoptotic phases was measured to be 2.69%, 10.29%, 16.92%, and 51.6%, respectively, which suggests that complex **2** can indeed induce apoptosis in SMMC7721 cells.

3.5.2. Cell cycle arrest

The cycle of SMMC7721 cells was investigated by flow cytometry after the said cells were treated with various concentrations of complex **2** (0, 1.5, and 3 μM) for 8 h. As can be evinced from the data reported in **Fig. 7**, with respect to the control (0 μM of complex **2**), the percentage of SMMC7721 cells in the G0-G1 phase increased from 38.73% to 42.28% and 53.24%, after treatment with complex **2** (1.5 and 3 μM, respectively). Meanwhile, as the concentration of the complex **2** used to treat the cells increased, the percentage of cells in the G2-M phase and in the S phase decreased. These results indicate that complex **2** can disturb DNA synthesis and ultimately arrest the cell cycle at the G0-G1 phase in a concentration-dependent manner.

3.5.3. Detection of mitochondrial membrane potential

Dissipation of the electrostatic potential across the mitochondrial membrane is one of the key hallmarks of mitochondrial dysfunction [38]. Rh123 is widely used to detect mitochondrial membrane potential. As can be evinced from the data in **Fig. 8**, the Rh123 fluorescence intensity decreased when cells were treated with complex **2**, indicating that the mitochondrial membrane potential had decreased and that mitochondrial activity had been impaired.

3.5.4. Cellular ATP production and Ca^{2+} level

Mitochondria are the cell's energy factories, which can participate in the synthesis of ATP, the primary energy source of cellular processes in living organisms [39–40]. Mitochondria also mediate Ca^{2+} uptake into the matrix to regulate metabolism, cell death, and cytoplasmic Ca^{2+} signaling. Mitochondrial dysfunction is always accompanied by ATP depletion in the cell and the Ca^{2+} leakage from the mitochondria into the cell cytoplasm [41]. As can be evinced from the data in **Fig. 9**, complex **2** induces a substantial dose-dependent decrease in intracellular ATP

levels. The intracellular Ca^{2+} level was determined using a fluorescent probe, Fluo-3/AM, by flow cytometry. As indicated by the data reported in **Fig. 10**, complex **2** treated cells displayed higher fluorescence intensity than control cells, indicating that vast amounts of Ca^{2+} ions had leaked out of the mitochondria.

4. Conclusions

Complexes **1** and **2** were designed, synthesized, and characterized. The complex containing the mitochondrion-targeting TPP group displayed enhanced cytotoxicity and cellular uptake compared with its TPP-free counterpart. Additionally, although complex **2**, which comprises TPP, was observed to bind DNA by intercalation thus disturbing DNA's secondary structure, its binding affinity toward DNA was observed to be marginally lower than that of complex **1**, which does not have a TPP moiety. The anticancer properties of the TPP-containing complex **2** were then investigated. Evidence indicated that complex **2** arrested the cell cycle at the G0-G1 phase. This complex disrupted mitochondrial structure, which potentially led to the simultaneous mitochondrial membrane collapse, ATP depletion in the cell, and Ca^{2+} leakage from the mitochondria into the cell cytoplasm, and eventually inducing cell apoptosis. Results thus indicated that the biological activity and cytotoxicity of the copper complex were markedly influenced by the presence of TPP acting as a mitochondrion-targeting group.

Acknowledgements

We gratefully acknowledge financial support by the National Natural Science Foundation of China (Nos. 21371046 and 21401041), and Key scientific research project plan of Colleges and Universities in He'nan province (19A150017), the Funding Program for Academic Technology Leaders of the He'nan University of Urban Construction (No. YCJXSJSDTR201705).

A. supplementary data

Crystallographic data for structural analysis have been deposited with the Cambridge Crystallographic Data Center, CCDC reference numbers 1959672–1959673. These data can be

obtained free of charge via www.ccdc.cam.ac.uk/conts/retrieving.htm (or from the Cambridge Crystallographic Data Center, 12 Union Road, Cambridge CB2 1EZ, UK; Fax: +44 1223 336033).

References

[1] J. Zielonka, J. Joseph, A. Sikora, M. Hardy, O. Ouari, J. Vasquez-Vivar, G. Cheng, M. Lopez, B. Kalyanaraman, Mitochondria-Targeted Triphenylphosphonium-Based Compounds: Syntheses, Mechanisms of Action, and Therapeutic and Diagnostic Applications, **Chem. Rev.**, 117 (2017) 10043–10120.

[2] J.H. Kang, Y.T. Ko, Enhanced Subcellular Trafficking of Resveratrol Using Mitochondriotropic Liposomes in Cancer Cells, **pharmaceutics**, 11 (2019) 423–440.

[3] X.H. Wang, H.S. Peng, L. Yang, F.T. You, F. Teng, A.W. Tang, F.J. Zhang, X.H. Li, Poly-L-lysine assisted synthesis of core–shell nanoparticles and conjugation with triphenylphosphonium to target mitochondria, **J. Mater. Chem. B.**, 1 (2013) 5143–5152

[4] M.A. Keibler, T.M. Wasylenko, J.K. Kelleher, O Iliopoulos, M.G.V Heiden, G. Stephanopoulos, Metabolic requirements for cancer cell proliferation, **Cancer Metab.**, 4 (2016)

[5] Z.G. Chen, X.X. Kang, Y.X. Wu, H.H. Xiao, X.Z. Cai, S.H. Sheng, X.F. Wang, S.G. Chen, A Mitochondria Targeting Artesunate Prodrug Loaded Nanoparticle Exerting Anticancer Activity via Iron-Mediated Generation of Reactive Oxygen Species, **Chem. Commun.**, 55 (2019) 4781–4784.

[6] K. Wang, C.C. Zhu, Y.F. He, Z.Q. Zhang, W. Zhou, N. Muhammad, Y. Guo, X.Y. Wang, Z.J. Guo, Restraining Cancer Cells by Dual-Metabolic Inhibitions with a Mitochondrion-Targeted Platinum(II) Complex, **Angew. Chem. Int. Edit.**, 58 (2019) 4638–4643.

[7] M.P. Chrysouli, C.N. Banti, N. Kourkoumelis, N. Panayiotou, A.J. Tasiopoulos, S.K. Hadjikakou, Chloro(triphenylphosphine)gold(I) a forefront reagent in gold chemistry as apoptotic agent for cancer cell, **J. Inorg. Biochem.**, 179 (2018) 107–120.

[8] A.D. Nisi, C. Bergamini, M. Leonzio, G. Sartor, R. Fato, M. Naldi, M. Monari, N. Calonghi, M. Bandini, Synthesis, cytotoxicity and anticancer activity of new alkynyl-gold(I) complexes, **Dalton Trans.**, 45 (2016) 1546–1553.

[9] R. Saez, J. Lorenzo, M.J. Prieto, M. Font-Bardia, T. Calvet, N. Omenaca, M. Vilaseca, V. Moreno, Influence of PPh_3 moiety in the anticancer activity of new organometallic ruthenium complexes, **J. Inorg. Biochem.**, 136 (2014) 1–12.

[10] A. Castonguay, C. Doucet, M. Juhas, D. Maysinger, New Ruthenium(II)-Letrozole Complexes as Anticancer Therapeutics, **J. Med. Chem.**, 55 (2012) 8799–8806.

[11] S.X. Jin, Y.G. Hao, Z.Z Zhu, N. Muhammad, Z.Q. Zhang, K. Wang, Y. Guo, Z.J. Guo, X.Y. Wang, Impact of Mitochondrion-Targeting Group on the Reactivity and Cytostatic Pathway of Platinum(IV) Complexes, **Inorg. Chem.**, 57 (2018) 11135–11145.

[12] C. Santini, M. Pellei, V. Gandin, M. Porchia, F. Tisato, C. Marzano, Advances in Copper Complexes as Anticancer Agents, **Chem. Rev.**, 114 (2014) 815–862.

[13] H.Y. Zhang, F. Xie, M.H. Cheng, F.Y. Peng, Novel Meta-iodobenzylguanidine-based Copper Thiosemicarbazide-1-guanidinomethyl-benzyl Anticancer Compounds Targeting Norephinephrine Transporter in Neuroblastoma, **J. Med. Chem.**, 62 (2019) 6985–6991.

[14] J.S. Zhang, J.Y. Hu, K. Peng, W. Song, S.C. Zhi, E.D. Yang, J.A Zhao, H.W. Hou, Chemical biology suggests pleiotropic effects for a novel hexanuclear copper(ii) complex inducing apoptosis in hepatocellular carcinoma cells, **Chem. Commun.**, 55 (2019) 11944–11947.

[15] W. Zhou, X.Y. Wang. M. Hu. C.C. Zhu, Z.J. Guo, A mitochondrion-targeting copper complex exhibits potent cytotoxicity against cisplatin resistant tumor cells through multiple mechanisms of action, **Chem. Sci.**, 5 (2014) 2761–2770.

[16] I. Papazoglou, P.J. Cox, A.G. Hatzidimitriou, C. Kokotidou, T. Choli-Papadopoulou, P. Aslanidis, Copper(I) halide complexes of 5-carbethoxy-2-thiouracil: Synthesis, structure and in vitro cytotoxicity, **Eur. J. Med. Chem.,** 78 (2014) 383–391.

[17] T.S. Morais, Y. Jousseaumea, M.F.M. Piedadeb, C. Roma-Rodriguesd, A.R. Fernandesd, F. Marquese, M.J.V. Brito, M.H Garciaa, Important cytotoxic and cytostatic effects of new Copper(I)-phosphane compounds with NN, NO and NS bidentate ligands, **Dalton Trans.**, 47 (2018) 7819–7829.

[18] W. Villarreal, L. Colina-Vegas, G. Visbal, O. Corona, R.S. Correa, J. Ellena, M.R. Cominetti, A.A. Batista, M. Navarro, Copper(I)-Phosphine Polypyridyl Complexes: Synthesis, Characterization, DNA/HSA Binding Study, and Antiproliferative Activity, **Inorg. Chem.**, 6 (2017) 3781–3793.

[19] K.M. Foote, J.W.M. Nissink, T.M. McGuire, P. Turner, S. Guichard, J.T. Yates, A. Lau, K. Blades, D. Heathcote, R. Odedra, G. Wilkinson, Z. Wilson, C. Wood, P.J. Jewsbury, Discovery and characterization of AZD6738, a potent inhibitor of ataxia telangiectasia mutated and rad3 related (ATR) kinase with application as an anticancer agent, **J. Med. Chem.**, 61 (2018) 9889–9907.

[20] A. Grillot, A.L. Tiran, D, Shannon, E, Krueger, Y.S. Liao, H. O'Dowd, Q.Tang, S. Ronkin, T.S. Wang, N. Waal, P. Li, D. Lauffer, E. Sizensky, J. Tanoury, E. Perola, T. H. Grossman, T. Doyle, B. Hanzelka, S. Jones, V. Dixit, N. Ewing, S.K. Liao, B. Boucher, M. Jacobs, Y. Bennani, P.S. Charifson, Second-Generation Antibacterial Benzimidazole Ureas: Discovery of a Preclinical Candidate with Reduced Metabolic Liability, **J. Med. Chem.**, 57 (2014) 8792–8816.

[21] H. Nimesh, S. Sur, D. Sinha, P. Yadav, P. Anand, P. Bajaj, J.S. Virdi, V. Tandon, Synthesis and Biological Evaluation of Novel Bisbenzimidazoles as Escherichia coli Topoisomerase IA Inhibitors and Potential Antibacterial Agents, **J. Med. Chem.**, 57 (2014) 5238–5257.

[22] J.A. Zhao, S.C. Zhi. H.B. Yu, R.N. Mao, J.Y. Hu, W. Song, J.S. Zhang, Mitochondrial and nuclear DNA dual damage induced by 2-(2'-quinolyl)benzimidazole copper complexes with potential anticancer activity, **RSC. Adv.**, 7 (2017) 51162–51174.

[23] O.V. Dolomanov, L.J. Bourhis, R.J. Gildea, J.A.K. Howard, H. Puschmann, OLEX2: a complete structure solution, refinement and analysis program, **J. Appl. Cryst.**, 42 (2009) 339–341.

[24] L. Krause, R. Herbst-Irmer, G.M. Sheldrick, D. Stalke, Comparison of silver and molybdenum micro focus X-ray sources for single-crystal structure determination, **J. Appl. Cryst.**, 48 (2015) 3–10.

[25] G.M. Sheldrick, Crystal structure refinement with SHELXL, **Acta Cryst.**, C71 (2015) 3–8.

[26] J. MARM UR, A Procedure for the Isolation of Deoxyribonucleic Acid from Micro -organismst, **J. Mol. Biol.**, 3 (1961) 208–218.

[27] M.E. Reichmann, S.A. Rice, C.A. Thomas, P. Doty, A Further Examination of the Molecular Weight and Size of Desoxypentose Nucleic Acid, **J. Am. Chem. Soc.**, 76 (1954) 3047–3053.

[28] A. Zianna, G.D. Geromichalos, A.G. Hatzidimitriou, E. Coutouli-Argyropoulou, M. Lalia-Kantouri, G. Psomas, Palladium(II) complexes with alicylaldehyde ligands: Synthesis, characterization, structure, in vitro and in silico study of the interaction with calf-thymus DNA and albumins, **J. Inorg. Biochem.**, 194 (2019) 85–96.

[29] A.W. Addison, T.N. Rao, J. Reedijk, J.V Rijn, G.C. Verschoor, Synthesis, Structure, and Spectroscopic Properties of Copper(II) Compounds containing Nitrogen-Sulphur Donor Ligands: the Crystal and Molecular Structure of

Aqua[l,7-bis(N-methylbenzimidazol-2'-yl)-2,6-dithiaheptane]copper(II) Perchlorate, **J. Chem. Soc. Dalton Trans.**, (1984) 1349–1356.

[30] L. Yang, D.R. Powell, R.P. Houser, Structural variation in copper(I) complexes with pyridylmethylamide ligands: structural analysis with a new four-coordinate geometry index, t_4, **Dalton Trans.**, (2007) 955–964.

[31] D.A. Safin, M. P. Mitoraj, K. Robeyns, Y. Filinchuk, C.M.L. Vande Velde, Luminescent mononuclear mixed ligand complexes of copper(I) with 5-phenyl-2,2′-bipyridine and triphenylphosphine, **Dalton Trans.**, 44 (2015) 16824‑16832.

[32] J.Y Lian, Q. Liu, Y. Jin, B.X. Li, Histone–DNA interaction: an effective approach to improve the fluorescence intensity and stability of DNA-templated Cu nanoclusters, **Chem. Commun.**, 53 (2017) 12568–12571.

[33] W.P. Roos, A.D. Thomas, B. Kaina, DNA damage and the balance between survival and death in cancer biology, **Nat. Rev. Cancer**, 16 (2016) 20–33.

[34] S. Kumar, R.P. Sharma, P. Venugopalan, V. Ferretti, S. Perontsis, G. Psomas, Copper(II) diclofenac complexes: Synthesis, structural studies and interaction with albumins and calf-thymus DNA, **J. Inorg. Biochem.**, 187 (2018) 97–108.

[35] Q. Cao, J. Yang, H. Zhang. L. Hao, G.G. Yang, L.N. Ji, Z.W. Mao, Traceable in-cell synthesis and cytoplasm-to-nucleus translocation of a zinc Schiff base complex as simple and economical anticancer strategy, **Chem. Commun.**, 55 (2019) 7852–7855.

[36] K.Q Qiu, Y. Chen, T.W. Rees, L.N. Ji, H. Chao, Organelle-targeting metal complexes: From molecular design to bio-applications, **Coord. Chem. Rev.**, 378 (2017) 66–86.

[37] X.C. Shi, Z.Y. Chen, Y.J. Wang, Z.J. Guo, X.Y. Wang, Hypotoxic copper complexes with potent anti-metastatic and anti-angiogenic activities against cancer cells, **Dalton Trans.**, 47 (2018) 5049–5054.

[38] J.D. Ly, D.R. Grubb, A. Lawen, The mitochondrial membrane potential ($\Delta\psi$m) in apoptosis; an update, **Apoptosis**, 8 (2003) 115–128.

[39] J.J. Deng, K. Wang, M. Wang, P. Yu, L.Q Mao, Mitochondria Targeted Nanoscale Zeolitic Imidazole Framework-90 for ATP Imaging in Live Cells, **J. Am. Chem. Soc.**, 139 (2017) 5877–5882.

[40] L. Hao, Z.W. Li, D.Y. Zhang, L. He, W.T. Liu, J. Yang, C.P. Tan, L.N. Ji, Z.W. Mao, Monitoring mitochondrial viscosity with anticancer phosphorescent Ir(III) complexes via two-photon lifetime imaging, **Chem. Sci.**, 10 (2019) 1285–1293.

[41] H. Vais, J.E. Tanis, M. Muller, R. Payne, K. Mallilankaraman, J.K. Foskett, MCUR1, CCDC90A, Is a Regulator of the Mitochondrial Calcium Uniporter, **Cell Metab.**, 22 (2015) 533–535.

Conflict of Interest

The authors declare no conflict of interest.

Figure

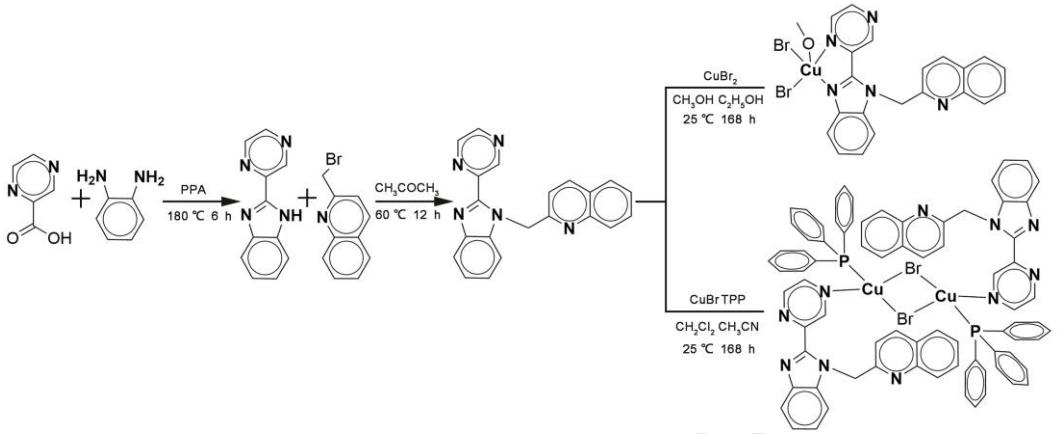

Scheme 1 Synthesis route to the ligand and complexes.

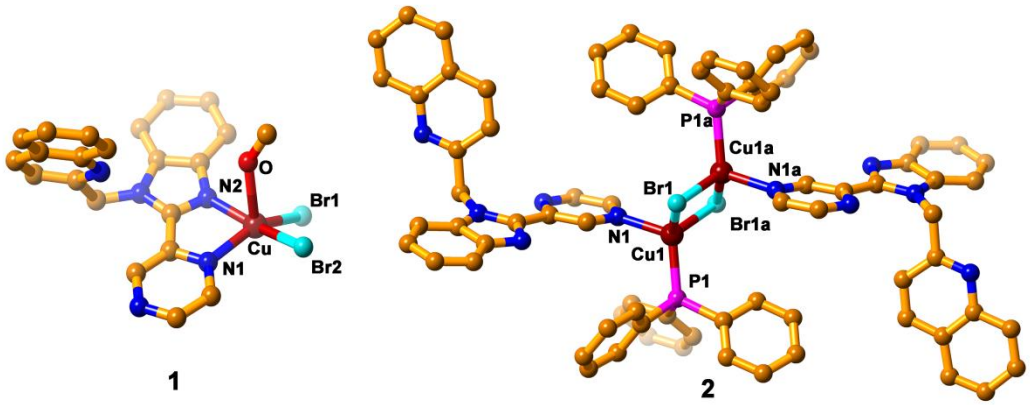

Fig. 1 Crystal structures of complexes **1** and **2**. Hydrogen atoms are omitted for clarity.

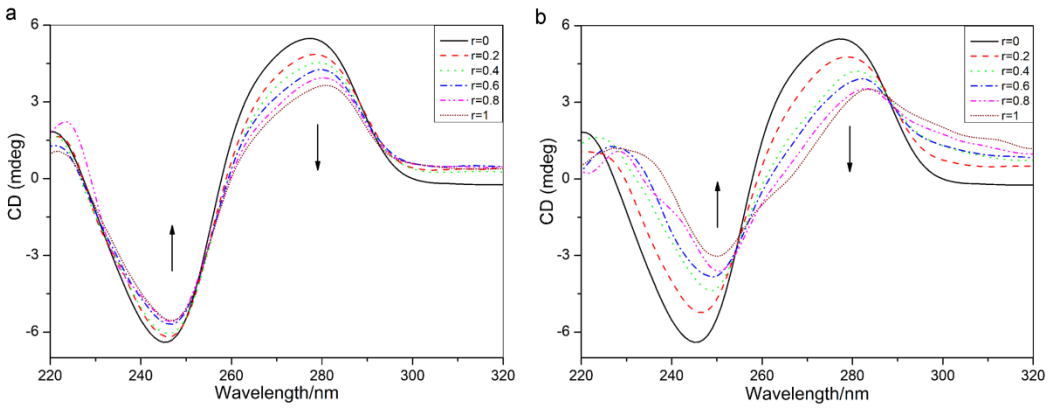

Fig. 2 The Circular dichroism spectral of CT-DNA in the absence and presence various concentrations of complexes. r = [complex]/[DNA] = 0, 0.2, 0.4, 0.6, 0.8, and 1 for complex **1** (a) and complex **2** (b), respectively.

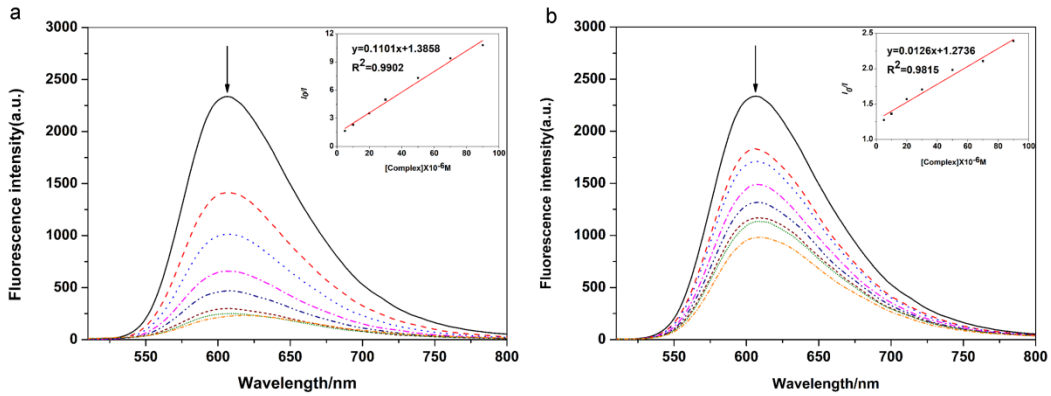

Fig. 3 The emission spectrum of EB-DNA in the absence and presence of various concentrations of complexes (0-90 μM). Conditions: [DNA] = 100 μM, [EB] = 10 μM for complex **1** (a) and complex **2** (b), respectively.

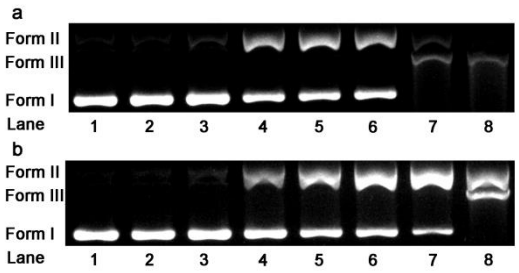

Fig. 4 The cleavage patterns of the agarose gel electrophoresis for pBR322 plasmid DNA by complex at 37 ° C for 4 h. Lane 1, DNA control; lane 2, DNA + ascorbic acid (1 mM) or H_2O_2 (1 mM); lane 3, DNA + complex (50 μM); lanes 4-8, DNA + ascorbic acid (1 mM) or H_2O_2 (1 mM) + complex (10, 20, 30, 40, and 50 μM, respectively) for complex **1** (a) and complex **2** (b), respectively.

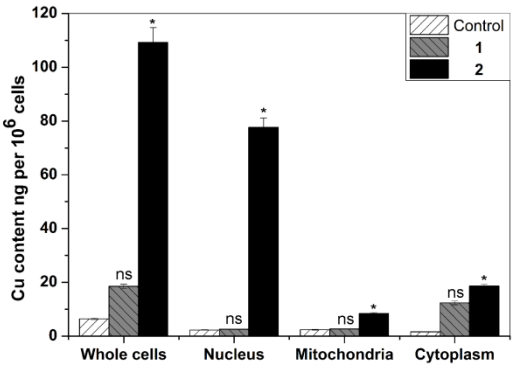

Fig. 5 Copper content (ng per10^6 cells) in SMMC7721 cells treated with complexes **1** (10 μM) and **2** (10 μM) for 8 h. Data are expressed as mean ± SD (n = 3), significant at the *p<0.05, **p<0.001, ***p<0.0001 levels using t-test, ns = not significant.

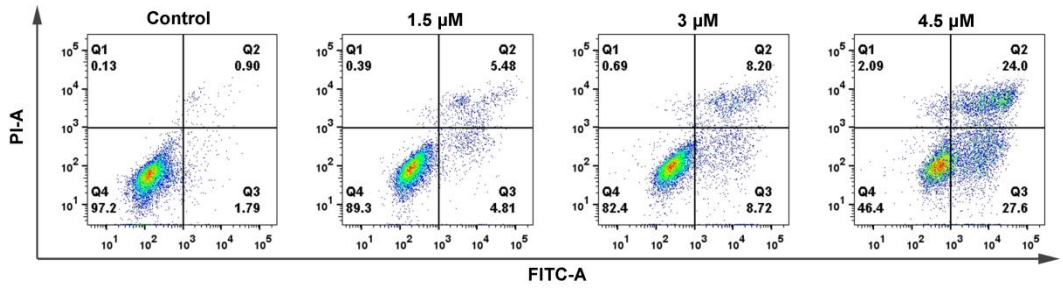

Fig. 6 Annexin V-PI assay of SMMC7721 cells treated with complex **2** at the indicated concentrations for 24 h.

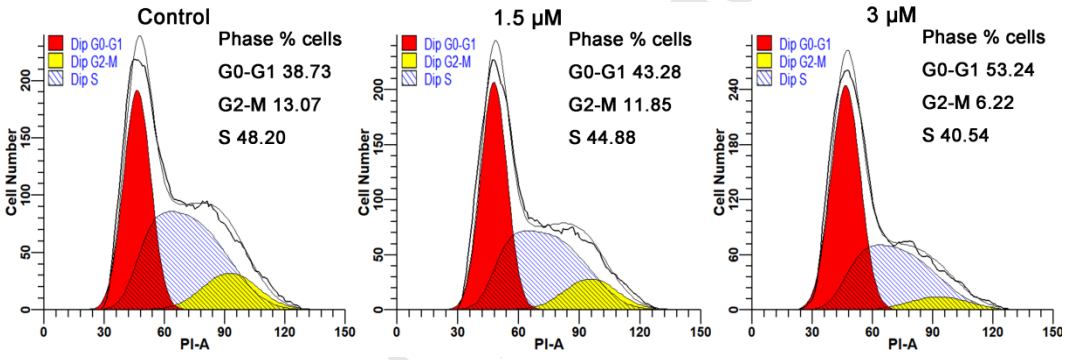

Fig. 7 The percentage of cell populations in different phases (G0-G1, G2-M, and S phase) in SMMC7721 cells treated by complex **2** for 8 h.

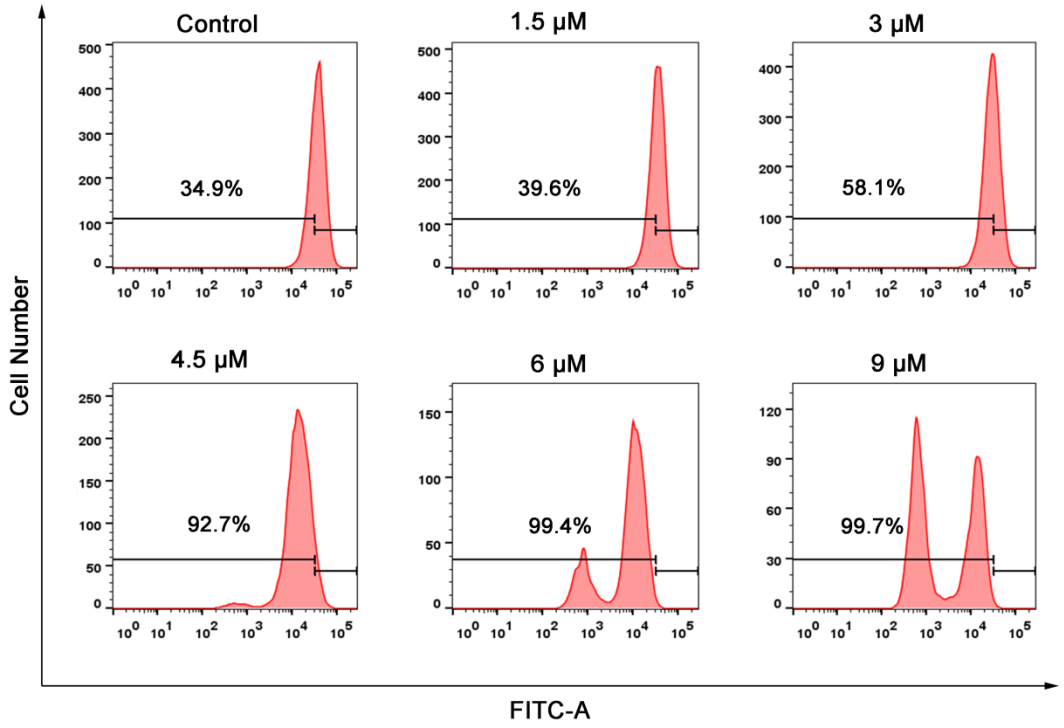

Fig. 8 Mitochondrial membrane potential changes in SMMC7721 cells after treatment with complex **2** at indicated concentrations for 8 h.

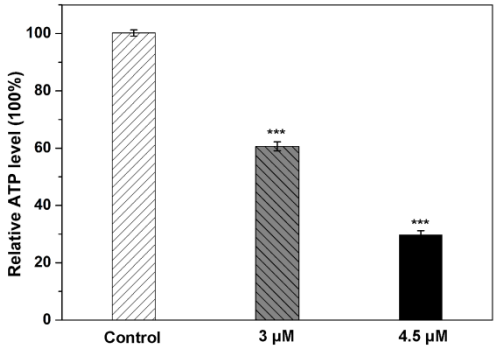

Fig. 9 Measurement of the intracellular level of ATP in the SMMC7721 cells after treatment with complex **2** at indicated concentrations for 24 h. Data are expressed as mean ± SD (n = 3), significant at the *p<0.05, **p<0.001, ***p<0.0001 levels using t-test.

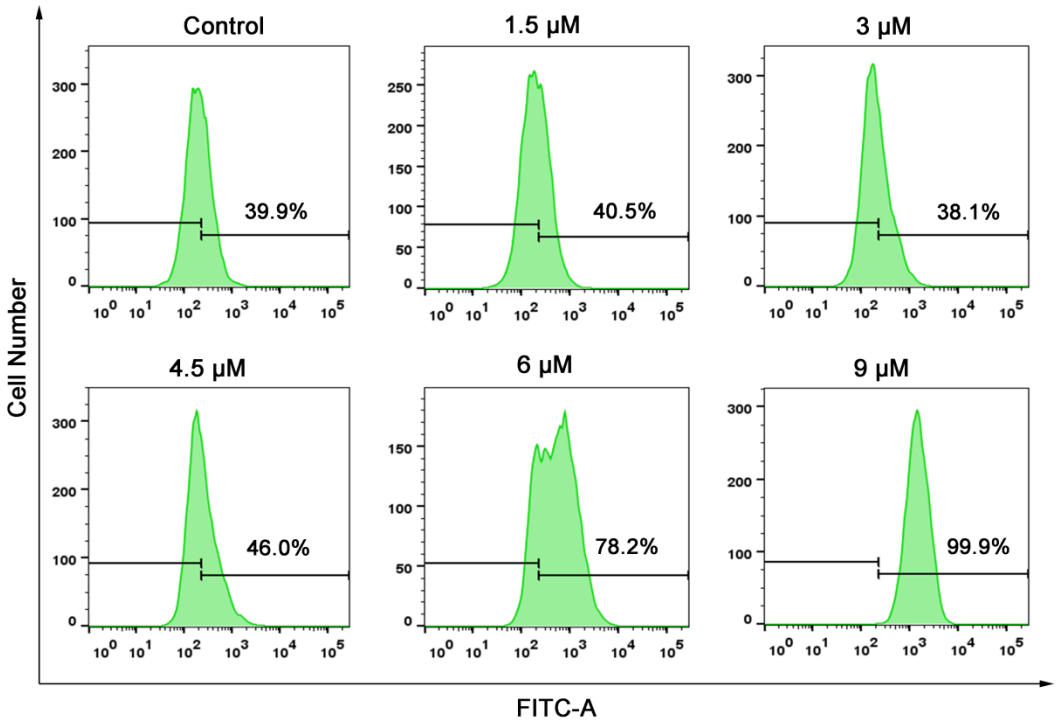

Fig. 10 Measurement of the intracellular level of Ca^{2+} in the SMMC7721 cells after treatment with complex **2** at indicated concentrations for 8 h using Fluo-3/AM as a fluorescent probe.

Table

Table 1. Crystallographic data and structural refinement for complexes **1**–**2**

Complex	**1**	**2**
Formula	$C_{22}H_{19}Br_2CuN_5O$	$C_{78}H_{60}Br_2Cu_2N_{10}P_2$
Mr.	592.78	1486.20
Temp(K)	160.01(10)	293(2)
λ (Cu, Kα), Å	1.54184	1.54184
Crystal system	triclinic	triclinic
Space group	*p*-1	*p*-1
a (Å)	9.8905(3)	9.1643(5)
b (Å)	10.9649(5)	13.2742(7)
c (Å)	11.4064(5)	15.1011(6)
α(deg)	74.934(4)	72.694(4)
β(deg)	71.276 (3)	84.863(4)
γ(deg)	87.274(3)	69.851(5)
Volume($Å^3$)	1118.46(9)	1646.45(15)
Z	2	1
F(000)	586.0	756.0

2θ range for data collection (°)	8.564–146.284	6.13–146.708
Goodness-of-fit on F^2	1.078	1.041
Final R indexes [$I > 2\sigma(I)$]	$R_1 = 0.0421$, $wR_2 = 0.1131$	$R_1 = 0.0284$, $wR_2 = 0.0751$

Table 2. Selected bond lengths (Å) and angles (°) for complexes **1**–**2**

1			
Cu(1)–Br(1)	2.3776(5)	Cu(1)–N(1)	2.072(3)
Cu(1)–Br(2)	2.3444(5)	Cu(1)–N(2)	1.991(3)
Cu(1)–O(1)	2.287(5)	N(1)–Cu(1)–Br(1)	147.03(7)
Br(2)–Cu(1)–Br(1)	96.20(2)	N(2)–Cu(1)–N(1)	79.37(10)
N(2)–Cu(1)–Br(2)	163.22(8)	N(2)–Cu(1)–Br(1)	96.90(8)
N(1)–Cu(1)–Br(2)	95.11(7)	N(1)–Cu(1)–O(1)	100.3(2)
O(1)–Cu(1)–Br(2)	86.75(14)	O(1)–Cu(1)–Br(1)	111.1(2)
2			
Cu(1)–Br(1)	2.4769(4)	Cu(1)–N(1)	2.0720(14)
Cu(1)–P(1)	2.2087(5)	Cu(1)–Cu(1a)	2.7896(5)
Cu(1a)–Br(1)	2.5362(3)	Br(1)–Cu(1)–Br(1a)	112.387(11)
P(1)–Cu(1)–Br(1)	118.019(16)	P(1)–Cu(1)–Br(1a)	109.793(15)
N(1)–Cu(1)–Br(1)	102.40(4)	N(1)–Cu(1)–P(1)	110.57(5)

Table 3. IC_{50} (μM) values of the tested complexes towards different cell lines over 48 h with cisplatin as the reference.

Complex	IC_{50} values (μM)			
	SMMC7721	BGC823	TFK-1	L-02
1	25.99 ± 1.75	25.45 ± 4.47	23.42 ± 2.31	42.47 ± 1.64
2	3.18 ± 0.09	3.61 ± 0.07	3.76 ± 0.28	11.90 ± 0.81
2-pbmq	>100	>100	>100	>100
Cisplatin	7.71 ± 0.31	4.66 ± 0.17	16.71 ± 1.73	8.66 ± 0.99

Table 4. UV-Vis absorbance of complexes **1** and **2** at 233 nm in water and 1-octanol at different concentrations and the corresponding lipophilicity (log *P*o/w).

Complex	Concentration (μM)	Ab_{water}		$Ab_{octanol}$	$\log P_{o/w}$	
		Before shaking	After shaking			
1	30	0.3488	0.1065	0.2423	0.36	0.46
	40	0.5058	0.1237	0.3821	0.49	
	50	0.7358	0.1685	0.5673	0.52	
2	30	1.9483	0.1138	1.8300	1.19	1.24
	40	2.6092	0.1381	2.4711	1.25	
	50	3.0560	0.1486	2.9074	1.29	

Graphical Abstract

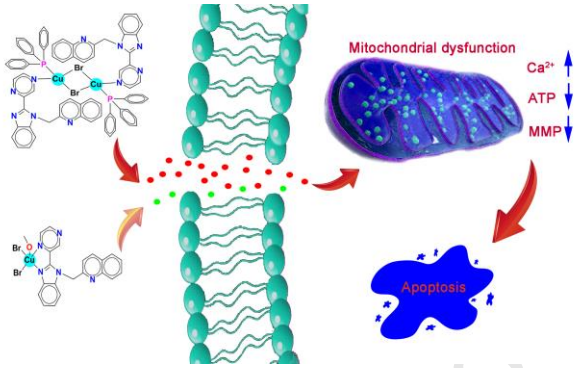

The complex containing triphenylphosphine displayed prominent cytotoxicity and cellular uptake compared with its triphenylphosphine-free counterpart. The complex possessing triphenylphosphine arrested the cell cycle at the G0-G1 phase, causing mitochondrial dysfunction involving simultaneous mitochondrial membrane potential collapse, ATP depletion and Ca^{2+} leakage, and eventually inducing cell apoptosis.

Highlihgts

1. Synthesis of Cu complex incorporating benzimidazole-quinoline and triphenylphosphine.

2. Increase of the lipophilicity and cytotoxicity by the introduction of triphenylphosphine.

3. Cause mitochondrial dysfunction involving mitochondrial membrane collapse, adenosine triphosphate depletion, and Ca^{2+} leakage.

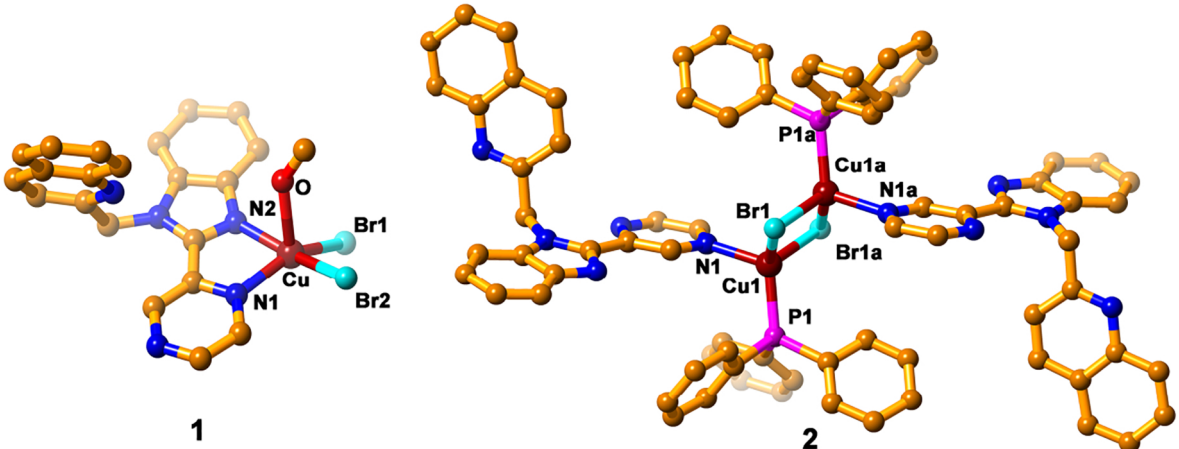

Figure 1

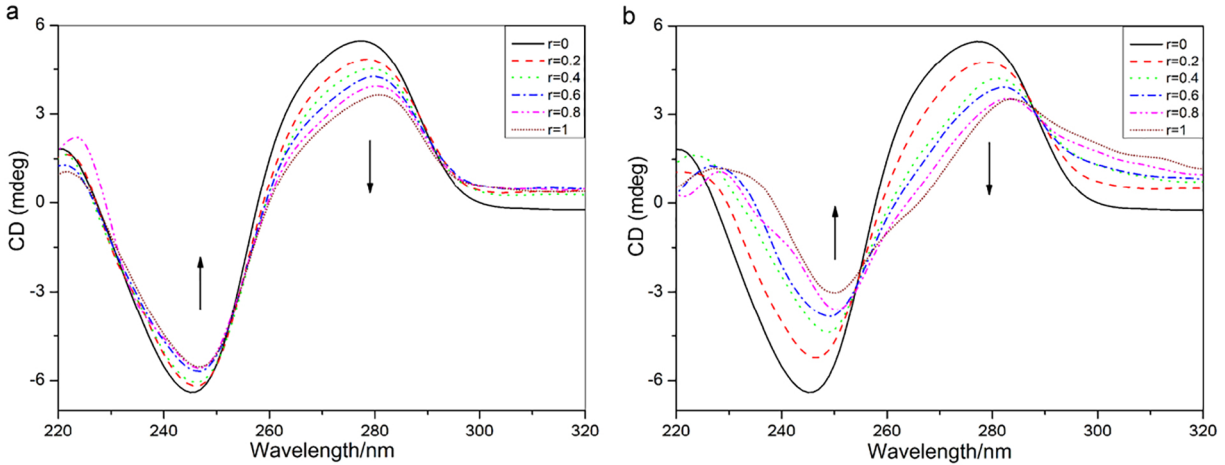
a
b
r=0
r=0.2
r=0.4
r=0.6
r=0.8
r=1
CD (mdeg)
Wavelength/nm
6
3
0
-3
-6
220
240
260
280
300
320

Figure 2

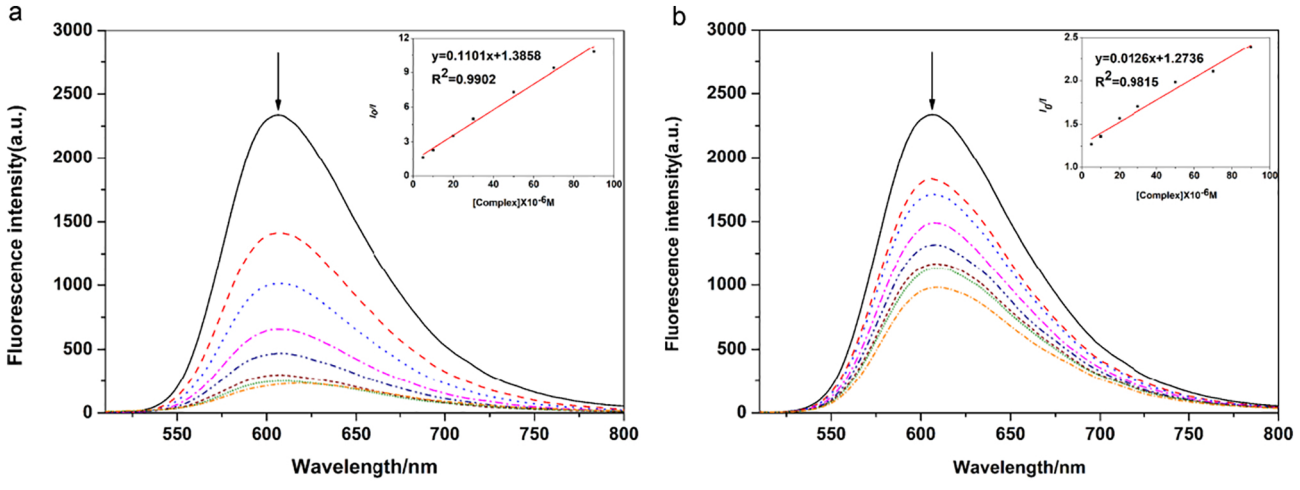
a
Fluorescence intensity(a.u.)
Wavelength/nm
y=0.1101x+1.3858
R2=0.9902
I0/I
[Complex]X10-6M
b
Fluorescence intensity(a.u.)
Wavelength/nm
y=0.0126x+1.2736
R2=0.9815
I0/I
[Complex]X10-6M

Figure 3

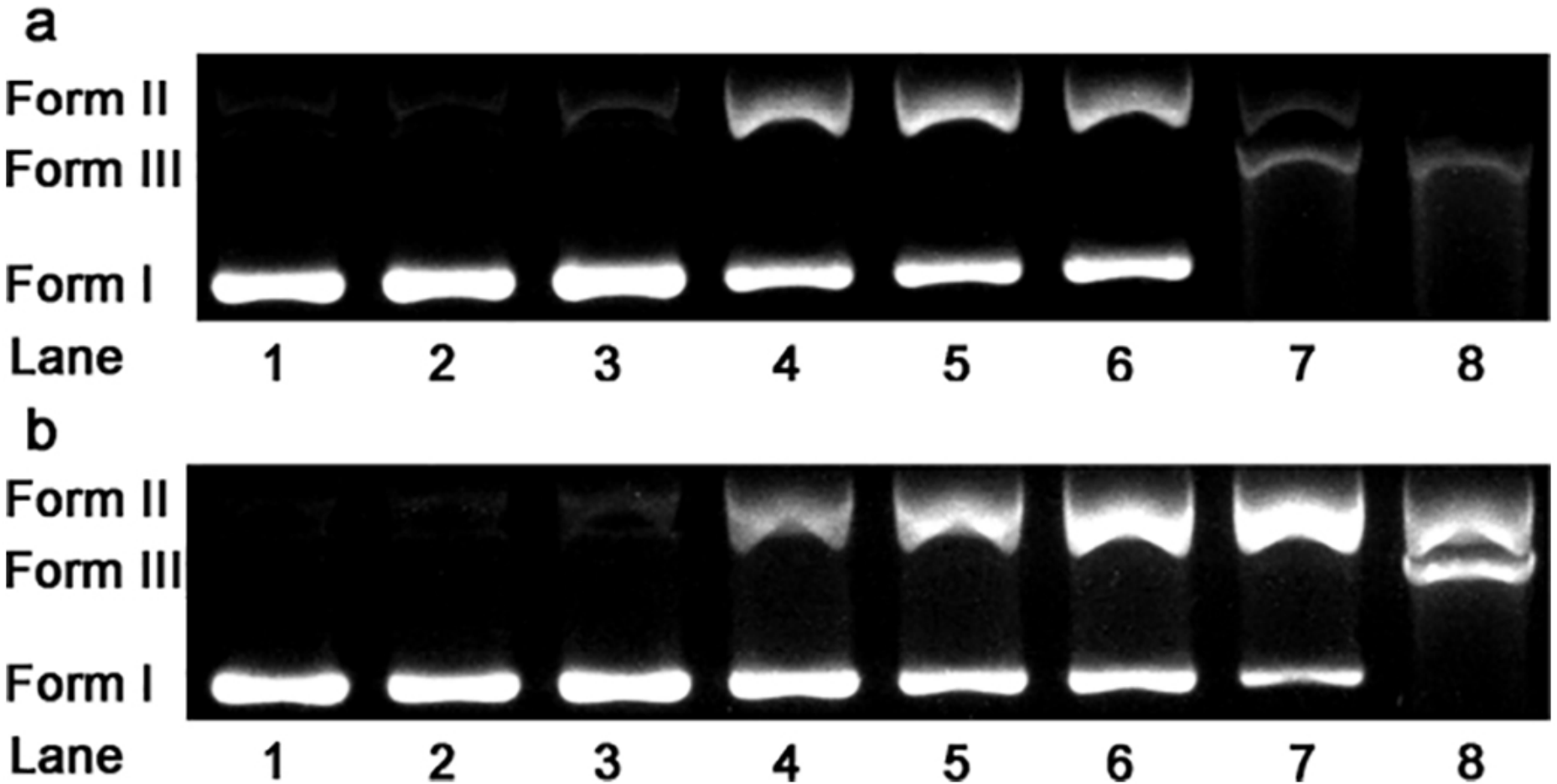
a
Form II
Form III
Form I
Lane
1
2
3
4
5
6
7
8
b
Form II
Form III
Form I
Lane
1
2
3
4
5
6
7
8

Figure 4

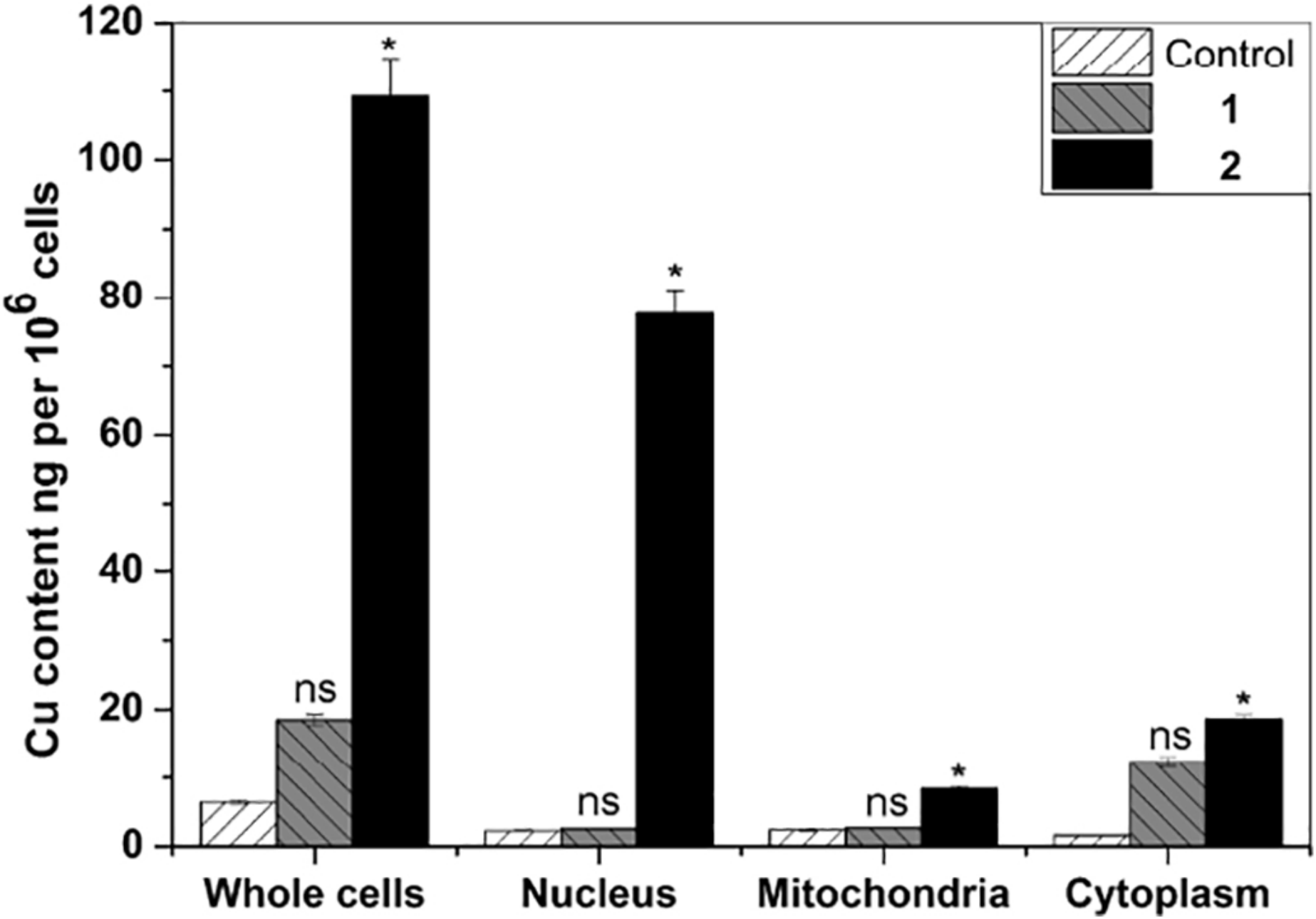
Control
1
2
Cu content ng per 10^6 cells
120
100
80
60
40
20
0
*
*
ns
ns
ns
*
ns
*
Whole cells
Nucleus
Mitochondria
Cytoplasm

Figure 5

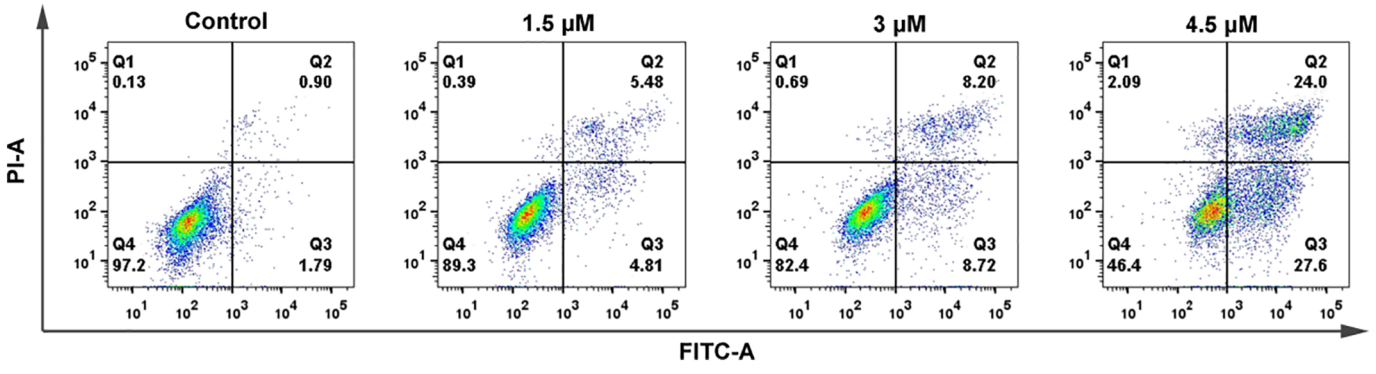
Control
1.5 μM
3 μM
4.5 μM
Q1
0.13
Q2
0.90
Q4
97.2
Q3
1.79
Q1
0.39
Q2
5.48
Q4
89.3
Q3
4.81
Q1
0.69
Q2
8.20
Q4
82.4
Q3
8.72
Q1
2.09
Q2
24.0
Q4
46.4
Q3
27.6
PI-A
FITC-A

Figure 6

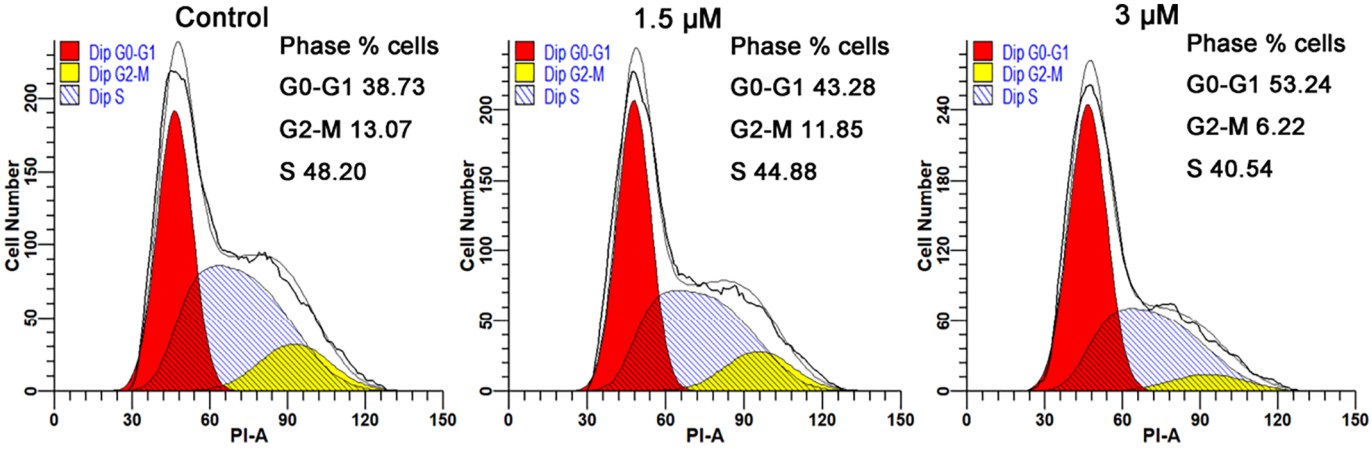
Control
Dip G0-G1
Dip G2-M
Dip S
Phase % cells
G0-G1 38.73
G2-M 13.07
S 48.20
Cell Number
PI-A
1.5 µM
Dip G0-G1
Dip G2-M
Dip S
Phase % cells
G0-G1 43.28
G2-M 11.85
S 44.88
Cell Number
PI-A
3 µM
Dip G0-G1
Dip G2-M
Dip S
Phase % cells
G0-G1 53.24
G2-M 6.22
S 40.54
Cell Number
PI-A

Figure 7

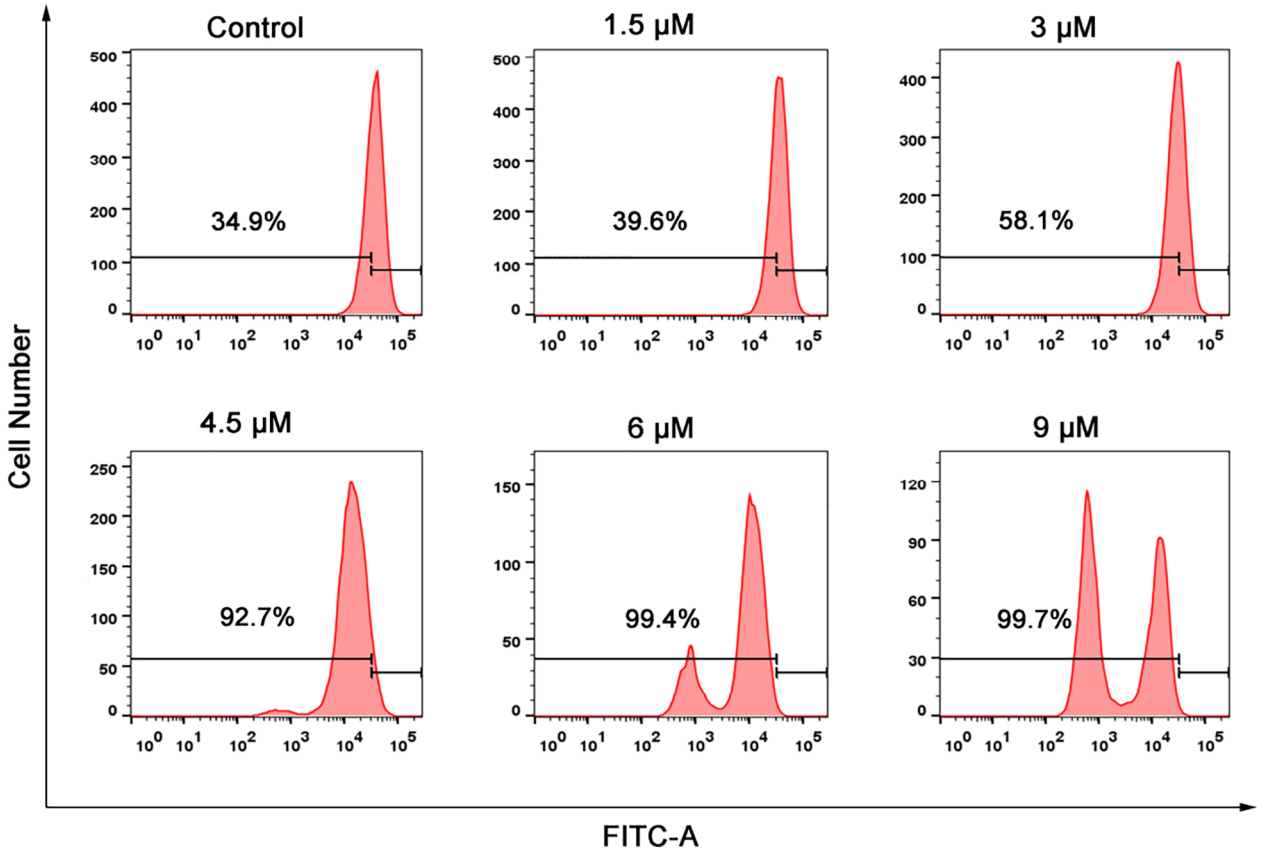
Control
1.5 μM
3 μM
4.5 μM
6 μM
9 μM
34.9%
39.6%
58.1%
92.7%
99.4%
99.7%
Cell Number
FITC-A

Figure 8

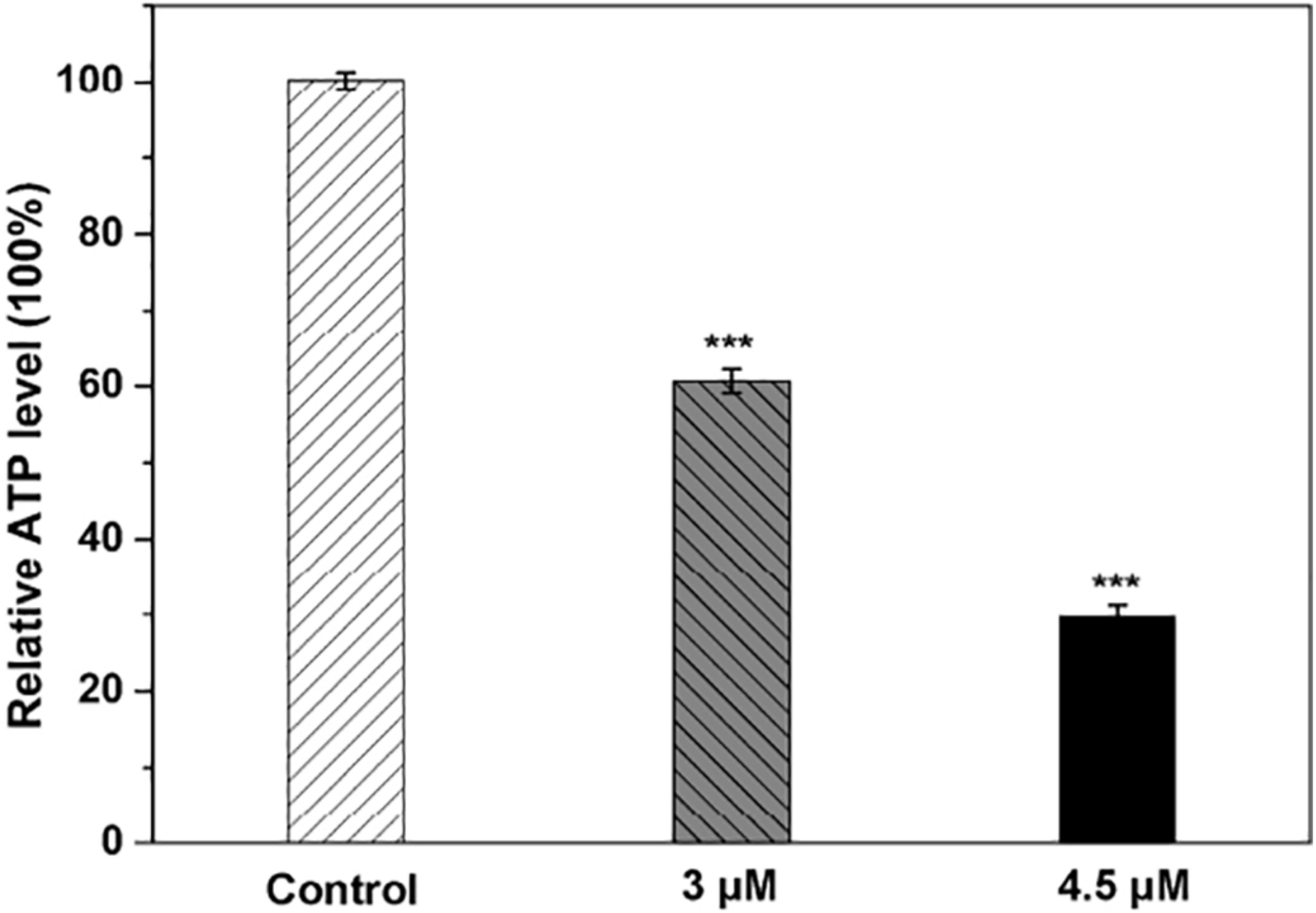

Figure 9

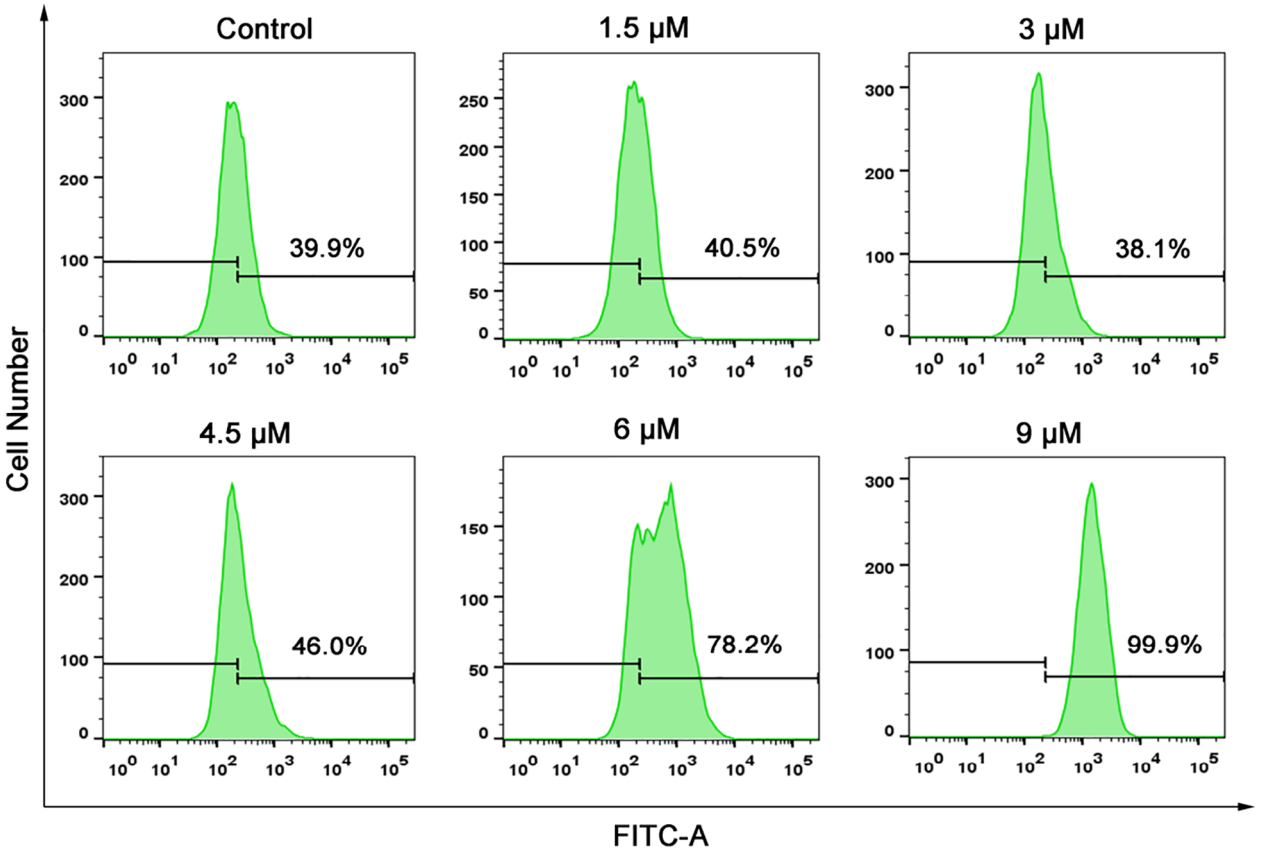
Control
1.5 μM
3 μM
4.5 μM
6 μM
9 μM
39.9%
40.5%
38.1%
46.0%
78.2%
99.9%
Cell Number
FITC-A

Figure 10